

A Computational Study on Ballistic Electronic Transport in Group-IV Armchair Nanoribbon Based Field Effect Transistors

Seyed Mohammad Tabatabaei^a, Kaveh Khaliji^a, Morteza Fathipour^a, Yaser Abdi^b, and Sara Fathipour^c

^a *School of Electrical and Computer Engineering, University of Tehran, Tehran, Iran, s.m.tabatabaei@ut.ac.ir*

^b *Department of Physics, University of Tehran, Tehran, Iran*

^c *Department of Electrical Engineering, University of Notre Dame, Indiana, USA*

Exploring novel alternative materials has become a major quest in the scientific community as we approach post-silicon nano-electronics. Extensive studies on graphene, an ultrathin carbon-based material, have revealed striking physical properties, potentially leading to brand-new solutions for contemporary electronic applications. Furthermore, silicene and germanene, the ultrathin buckled honeycomb structures of silicon and germanium (other group-IV elements of the periodic table), are recently predicted to be thermodynamically stable using density functional theory (DFT) calculations [1]. Compelling experimental evidence regarding the existence of silicene on metallic substrates have also been reported [2]. However, a common drawback among these sheets is the absence of bandgap which may be overcome by cutting them into nanoribbons with either armchair or zigzag edges (ANRs or ZNRs).

Our DFT calculations use the SIESTA code with a force relaxation constraint of 0.01 eV/Å [3]. The top-of-the-barrier (ToB) model [4] is employed to evaluate the ultimate performance of the intrinsic double gate field effect transistor (DGFET) shown in Fig. 1. This model accurately reproduces the results of rigorous quantum mechanical simulations based on the non-equilibrium Green's function (NEGF) formalism for channel lengths larger than 10 nm. In accordance with the perfect electrostatic control of the gate over the atomically thin channels considered in this work, C_S and C_D are assumed to be negligible (see Fig. 1(c)). We have taken advantage of the full band DOS obtained from DFT calculations in the ToB model, thereby directly assessing the influences of the first-principle band structures on device characteristics.

Based on their electronic properties, ANRs are categorized into three distinct families specified by $N_A = 3p + k$, where N_A is the number of dimer lines across the ribbon's width (see Fig. 1(b)), p is an integer, and $k=0, 1, 2$. In order to study the three families in each of the group IV-based ANRs, a comparison of the potential electronic characteristics under equal bandgap energy is carried out. However, due to the small bandgap in ANRs with $N_A = 3p+2$, this family is not suitable for digital logic applications and will not be investigated further. Therefore, we consider ANRs of $N_A = 12$ and 19 from AGNRs, $N_A = 24$ and 28 from ASiNRs, and $N_A = 6$ and 10 from AGeNRs. The results for carrier transit time versus V_{GS} for the three selected pairs are shown in Fig. 2(a), (b), and (c). Accordingly, carrier transit time exhibits a general descending behavior as the gate reduces the potential barrier in the channel by increasing V_{GS} . Moreover, increasing V_{GS} can change the subband which contributes most to the current. Hence, a local deceleration of carriers which is due to a rise in the effective mass of carriers may be observed (see Fig. 2(b)). In Fig. 2(d), (e), and (f), we have obtained the intrinsic delay versus I_{ON}/I_{OFF} ratio curves for the aforementioned three pairs of ANRs. The intrinsic delay is calculated as $\tau = (Q_{ON} - Q_{OFF})/I_{ON}$ where Q_{ON} and Q_{OFF} are the total charge in the channel at ON state and OFF state, respectively, and I_{ON} is the ON current. Using τ versus I_{ON}/I_{OFF} ratio for comparison, one can simultaneously consider the ON and OFF states and perform an assessment of the device characteristics independent of the channel's geometry. From Fig. 2(d), (e), and (f), it can be readily inferred that the $N_A = 3p$ family in all group-IV ANRs outperforms the $N_A = 3p+1$ family, in agreement with a previous study on AGNRs [5]. Eventually, in order to assess which of the group-IV ANRs possesses superior properties in terms of FET application, three ANRs of $N_A = 3p$ family with $E_{gap} \sim 0.4$ eV are investigated, i.e. 18-AGNR, 6-SiANR, and 6-GeANR. As shown in Fig. 3(a), the current drive of 18-AGNR is slightly higher than ANRs based on Si and Ge. The reason for this can be explained by referring to the results for quantum capacitance (C_Q) in Fig. 3(b). As can be seen, the calculated C_Q for 18-AGNR is comparable with C_{ox} while the obtained C_Q for 6-SiANR and 6-GeANR are much higher than C_{ox} . This is due to the considerably larger effective mass of electrons in 6-ASiNR and 6-AGeNR ($m^* \sim 0.45m_0$) which gives rise to a higher DOS and C_Q compared to 18-AGNR ($m^* \sim 0.05m_0$). As a result, for 6-SiANR and 6-GeANR,

gate will have a lower control over the carriers in the channel. Figure 3(c) shows that V_{GS} can significantly modulate the average electron velocity in the case of 18-AGNR, due to its comparable C_Q with C_{ox} . Finally, Fig. 4(d) shows that the intrinsic delay is deteriorated by at least 50% at I_{ON}/I_{OFF} ratio of about 10^5 for 6-SiANR and 6-GeANR.

In conclusion, it is found that FETs based on $N_A = 3p$ family of AGNRs are the most preferable, compared to other group-IV armchair nanoribbons, in terms of I_{ON}/I_{OFF} ratio, intrinsic device delay, and carrier transit time due to their smaller quantum capacitance (C_Q) which is attributed to the lighter electron effective mass in AGNRs compared to Ge and Si ANRs at the same bandgap energy.

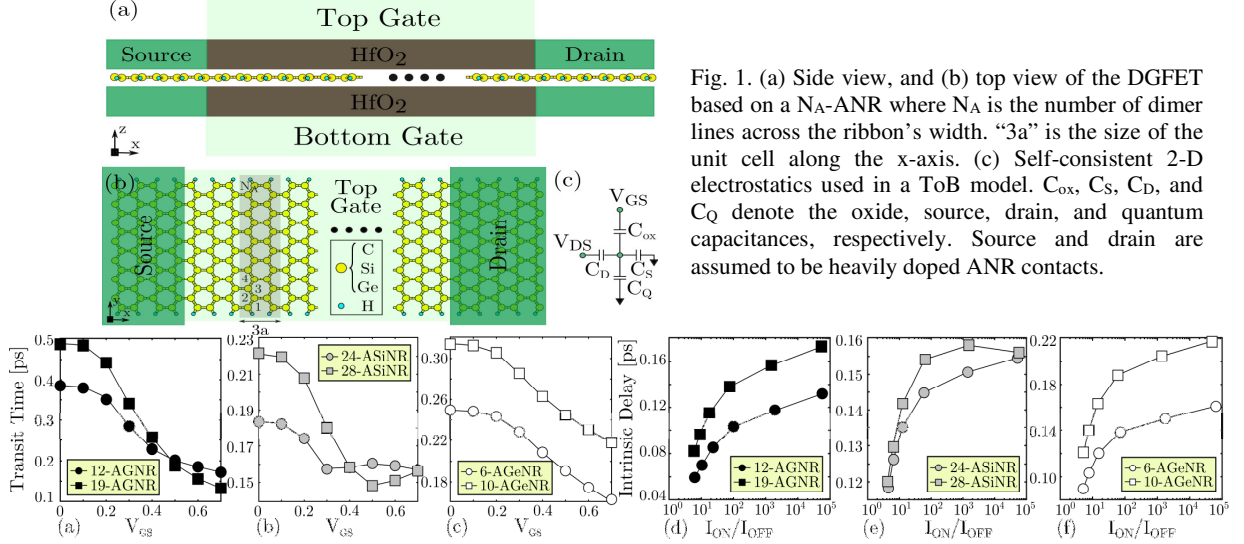


Fig. 1. (a) Side view, and (b) top view of the DG-FET based on a N_A -ANR where N_A is the number of dimer lines across the ribbon's width. "3a" is the size of the unit cell along the x-axis. (c) Self-consistent 2-D electrostatics used in a ToB model. C_{ox} , C_S , C_D , and C_Q denote the oxide, source, drain, and quantum capacitances, respectively. Source and drain are assumed to be heavily doped ANR contacts.

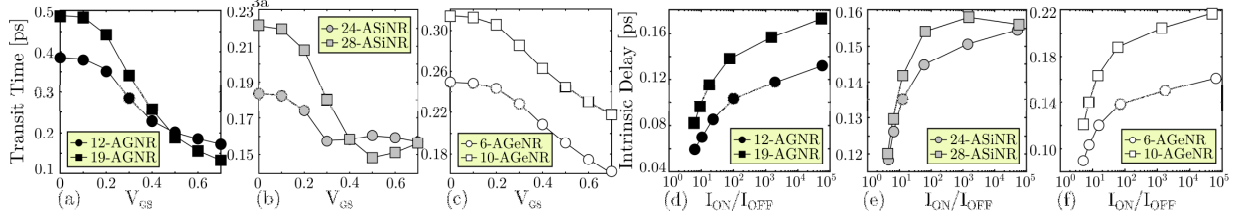


Fig. 2. (a), (b), and (c) are the carrier transit time versus V_{GS} for $N_A = 12$ and 19 AGNRs ($E_{gap} \sim 0.6$ eV), $N_A = 24$ and 28 ASiNRs ($E_{gap} \sim 0.14$ eV), and $N_A = 6$ and 10 -AGeNRs ($E_{gap} \sim 0.4$ eV), respectively. (d), (e), and (f) are the intrinsic device delay versus I_{ON}/I_{OFF} ratio for the same ANRs. The channel length is assumed to be 12 nm.

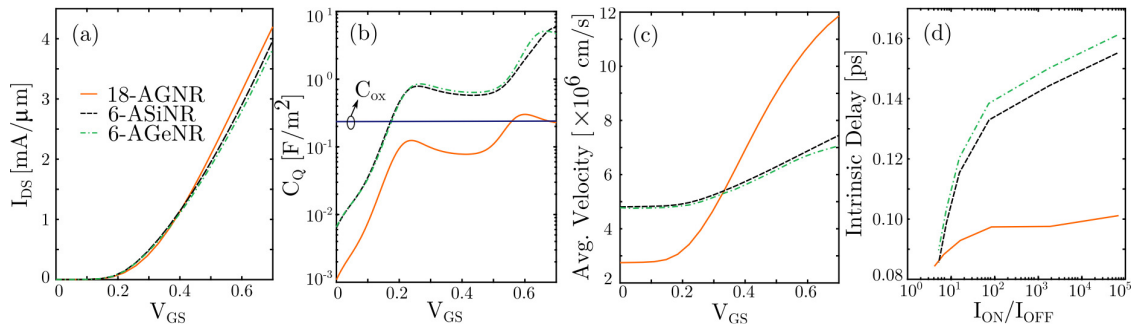


Fig. 2. (a) Transfer characteristic, (b) quantum capacitance, (c) average velocity, and (d) intrinsic device delay versus I_{ON}/I_{OFF} ratio for 6-SiANR, 6-GeANR, and 18-CANR all having $E_{gap} \sim 0.4$ eV. The quantum capacitance is calculated as $C_Q = \partial(qN)/\partial(-U_{scf}/q)$ where qN and U_{scf} are the charge density and the potential at the ToB, respectively. In (a), an OFF-current density equal to $0.06 \mu A/\mu m$ is assumed to provide a fair benchmarking. The horizontal dashed line in (b) represents the oxide capacitance given by $C_{ox} = \epsilon_{ox}/t_{ox}$. A 3-nm HfO_2 ($\kappa = 25$) is assumed.

References

- [1] E. Scalise, et al. "Vibrational properties of silicene and germanene," *Nano Research*, vol. 6, no. 1, pp. 19-28, (2013).
- [2] P. Vogt, et al. "Silicene: compelling experimental evidence for graphene like two-dimensional silicon," *Physical Review Letters*, vol. 108, p. 155501, Apr. (2012).
- [3] J. M. Soler, et al. "The SIESTA method for *ab initio* order-N materials simulation," *Journal of Physics: Condensed Matter*, vol. 14, no. 11, p. 2745, 2002.
- [4] A. Rahman, et al. "Theory of ballistic nanotransistors," *IEEE Transactions on Electron Devices*, vol. 50, no. 9, pp. 1853-1864, Sep. 2003.
- [5] R. Sako, et al. "Computational Study of Edge Configuration and Quantum Confinement Effects on Graphene Nanoribbon Transport," *IEEE Electron Device Letters*, vol. 32, pp. 6-8, 2011.